applied sciences

MDPI

Article

GLADE: Gravitational Light-Bending Astrometry Dual-Satellite Experiment

Mario Gai *, Alberto Vecchiato, Alberto Riva, Alexey G. Butkevich, Deborah Busonero and Federico Landini

INAF—Istituto Nazionale di Astrofisica, Osservatorio Astrofisico di Torino, Via Osservatorio 20, 10025 Pino Torinese, TO, Italy; alberto.vecchiato@inaf.it (A.V.); alberto.riva@inaf.it (A.R.); alexey.butkevich@inaf.it (A.G.B.)

* Correspondence: mario.gai@inaf.it

Abstract: Light bending is one of the classical tests of general relativity and is a crucial aspect to be taken into account for accurate assessments of photon propagation. In particular, high-precision astrometry can constrain theoretical models of gravitation in the weak field limit applicable to the Sun neighborhood. We propose a concept for experimental determination of the light deflection close to the Sun in the 10^{-7} to 10^{-8} range, in a modern rendition of the 1919 experiment by Dyson, Eddington and Davidson, using formation flying to generate an artificial long-lasting eclipse. The technology is going to be demonstrated by the forthcoming ESA mission PROBA3. The experimental setup includes two units separated by 150 m and aligned to the mm level: an occulter and a small telescope (0.3 m diameter) with an annular field of view covering a region 0°.7 from the Sun. The design is compatible with a space weather payload, merging several instruments for observation of the solar corona and environment. We discuss the measurement conditions and the expected performance.

Keywords: astrometry; catalogs; instrumentation; high angular resolution; methods; numerical; techniques; image processing

Citation: Gai, M.; Vecchiato, A.; Riva, A.; Butkevich, A.G.; Busonero, D.; Landini, F. GLADE: Gravitational Light-Bending Astrometry Dual-Satellite Experiment. *Appl. Sci.* **2024**, *14*, 888. https://doi.org/10.3390/app14020888

Academic Editor: Giulio Nicola Cerullo

Received: 14 December 2023
Revised: 11 January 2024
Accepted: 17 January 2024
Published: 20 January 2024

1. Introduction

The observation of known stellar fields by Dyson, Eddington and Davidson during the 1919 (29 May) eclipse brought confirmation of Einstein's general relativity (GR) theory into public awareness. It measured the apparent positions during the eclipse of a few stars, within a few degrees from the Sun, compared to their unperturbed relative positions. The concept is shown in Figure 1: the stars' true positions are marked in red, and their photons would follow the dashed lines if the Sun were not present; the space-time curvature induced by gravitation generates the curved photon trajectories (solid lines), so that the apparent star positions (in blue), seen by the observer on the straight (dotted) line prolongation of the incoming photon direction, are displaced away from the Sun.

The measured angular variation was interpreted in terms of light deflection, providing an estimate of the γ parameter of the parametrized post-Newtonian (PPN) formulation of gravity theories [1] with a precision of ∼10%. The current best estimate of γ, from a single pass of the Cassini probe behind the Sun, is in the 10^{-5} range [2]. The expectations for the Gaia mission [3], currently offering its Data Release 3 (DR3) catalog [4,5], are in the 10^{-6} range [6], after initial hopes of an even better photon limit [7].

We recall that, apart from the intrinsic value of fundamental physics, the implications for our modern technology are paramount; without GR taken into account, in fact, the clocks used in GPS satellites would be faster than nominally identical ground-based clocks by about 45 µs per day (partially mitigated by a 7 µs/day counter-effect from special relativity), resulting in ∼10 km of error accumulated each day (https://en.wikipedia.org/wiki/Error_analysis_for_the_Global_Positioning_System, accessed on 13 December 2023) [8].

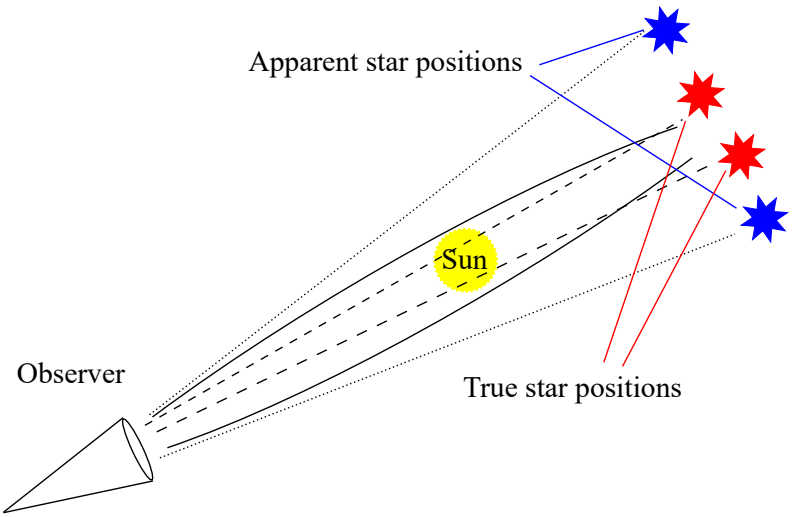

Figure 1. Light deflection of stellar photons by the Sun. True star positions (red) appear displaced away (blue) from the Sun since the real curved trajectories (solid lines) are interpreted as the tangential (dotted) straight lines at the observer.

The issue is partially mitigated by design, scaling the actual on-board clock rate to the correct average value; nonetheless, real-time corrections are still required to achieve the precision level we are used to relying on in everyday life, not to mention the most demanding applications (high-precision surveying, autonomous driving, and so on). With future developments of human activity in space, deployment of positioning systems on inter-planetary scale may be considered, with even more demanding needs for correct relativistic description [9].

Light deflection is an unavoidable first-order contribution to the complex trajectory of photons in the GR universe, affected by all gravitational sources and phenomena. In a simple framework [10], an observer at a distance d from the center of the Sun (mass $M_\odot$) will see a star outwardly displaced by an amount $\delta\varphi$ with respect to its unperturbed angle φ to the Sun:

$$\delta\varphi = (1+\gamma)\frac{G\,M_\odot}{c^2\,d}\cot(\varphi/2)\,. \tag{1}$$

The peak value at the Sun's limb is about $1''.75$, still retaining a non-negligible value for micro-arcsecond (hereafter, μas) astrometry over most of the sky: at 90° from the Sun, it is about 4 milli-arcsec (hereafter, mas). Gaia observes in a range of angular distance to the Sun $45^\circ \leqslant \varphi \leqslant 135^\circ$, where light deflection is in the range $9.8\,\text{mas} \geqslant \delta\varphi \geqslant 1.7$ mas, respectively.

The relevance of deflection measurement can be appreciated from the consideration that GR acts as a cosmological attractor for scalar–tensor gravitation theories, with expected deviations from unity of γ in the 10^{-5} to 10^{-7} range [11]. It is therefore crucial to improve the test precision by one or two orders of magnitude with respect to the state of the art in order to set significant physical constraints on acceptable gravity theories. Furthermore, it is worth stressing that we are referring here to the light deflection phenomenon due to the *local* curvature of spacetime, namely the curvature generated by the mass-energy of individual physical bodies, rather than the one associated with the cosmological evolution of the Universe [12–15]. It may be noted that, at this level of accuracy, the effects of the 2PN order might be significant; in this case, the PPN formulation should be extended to cast the interpretation of measurements in terms of the parametrized post-post-Newtonian (PPPN) framework.

Measurements of light deflection from the ground are affected by several shortcomings, such as short eclipse duration, high background flux from the Sun disk and inner solar corona, atmospheric disturbances and the limited number of bright sources in the field, thus limiting the achievable performance independently from near future technological improvements. We proposed a dedicated space experiment concept for high-precision

determination of the deflection close to the Sun by means of a custom instrument optimized for both coronagraphy (to reject the overwhelming solar flux) and large field astrometry, in the framework of the ESA's calls for medium-class missions M3 [16] and M4 [17].

Coronagraphy is a crucial tool of solar physics since the Sun's outer regions and their phenomena can only be observed by effectively masking the intense flux from the disk (and inner corona). In addition, energetic outbursts (e.g., solar flares) can induce severe damage to our orbital infrastructure [18], relying on hundreds of satellites devoted to telecommunications, weather monitoring, Earth observation and so on. The 1859 event [19] demonstrates that even the ground-based equipment of the time was liable to severe disruption, thus evidencing the criticality of present-day infrastructure with respect to space weather.

PROBA 3 [20] is the third mission of the European Space Agency (ESA) Project for On-Board Autonomy, planned for launch in 2024, which is aimed at demonstrating the feasibility of formation flying with the relative geometry of two independent spacecrafts at the sub-mm and arcsec level or better, respectively, on relative position and pointing accuracy over a 150 m distance. It will host the externally occulted solar coronagraph ASPIICS for observation of the solar corona at unprecedented spatial resolution and low altitude from the Sun disk, down to 1.1 $R_\odot$. This will also demonstrate the technology of interest to our purposes.

We propose the concept of a space mission devoted to fundamental physics and employing state-of-the-art astronomical techniques, in particular astrometry and coronagraphy, in order to assess the light deflection induced by the Sun's gravitational field. The Gravitational Light-bending Astrometry Dual-satellite Experiment (GLADE) takes advantage of the PROBA3 formation flying technology and the ASPIICS approach in splitting occulter and coronagraph units for astrometric measurements on stellar fields around the Sun, with the goal of high-precision determination of the light deflection predicted by general relativity and competing gravitation theories. This approach significantly mitigates the technical challenges involved in the previously proposed instrument concept [16,17].

In this paper, we briefly outline the mission concept in Section 2, its expected performance in Section 3, and the roadmap toward implementation in Section 4.

2. Materials and Methods

GLADE inherits most of the mission profile of PROBA3, in particular the occulter structure and the relative spacecraft geometry management throughout their orbits. We recall that the two satellites will fly together in a highly elliptic 19.6 h orbit and implement an artificial 6 h eclipse throughout the low-disturbances apogee phase, implementing a giant externally occulted coronagraph. ASPIICS will perform regular white-light observations of the solar corona in the radial range $1.1\,R_\odot \leqslant \rho \leqslant 3\,R_\odot$. The Occulter spacecraft has the basic function of keeping the occulting disk (diameter ∼1.4 m) at the desired ∼150 m distance from the Coronagraph spacecraft during observations, ensuring an unvignetted view of the corona above $1.17\,R_\odot$. The observing instrument is a refractive telescope equipped with an internal occulter and Lyot stop to mitigate the residual diffracted light from the external occulter; its resolution is limited by the entrance aperture diameter of 50 mm to a pixel angular scale of $2''.81$ on its $2k \times 2k$ CMOS detector.

GLADE relies on the same overall observing setup, modified in order to achieve higher angular resolution on a circular region around the Sun, thus optimizing the astrometric performance on the field stars. Better imaging resolution, projecting a smaller sky region on each pixel, generally improves astrometric precision [21,22] because a narrower photon distribution has a lower dispersion on a photo-center estimate, i.e., it is better localized. However, in our case, it also helps in reducing the background (from the solar corona and residual diffracted light from the Sun disk) collected by the smaller pixels.

Hereafter, we outline the instrument concept in Section 2.1, its operation in Section 2.2, and some of the key aspects of performance analysis in Section 2.3.

2.1. The Instrument

The GLADE reflecting telescope has a 0.3 m primary mirror, i.e., six times larger than the PROBA3 telescope. The instrument layout is shown in Figure 2: stellar photons proceed from the primary mirror (M1) to the secondary mirror (M2), then to the folding mirror (FM) and the tertiary mirror (M3), finally reaching the ring-shaped focal plane (FP).

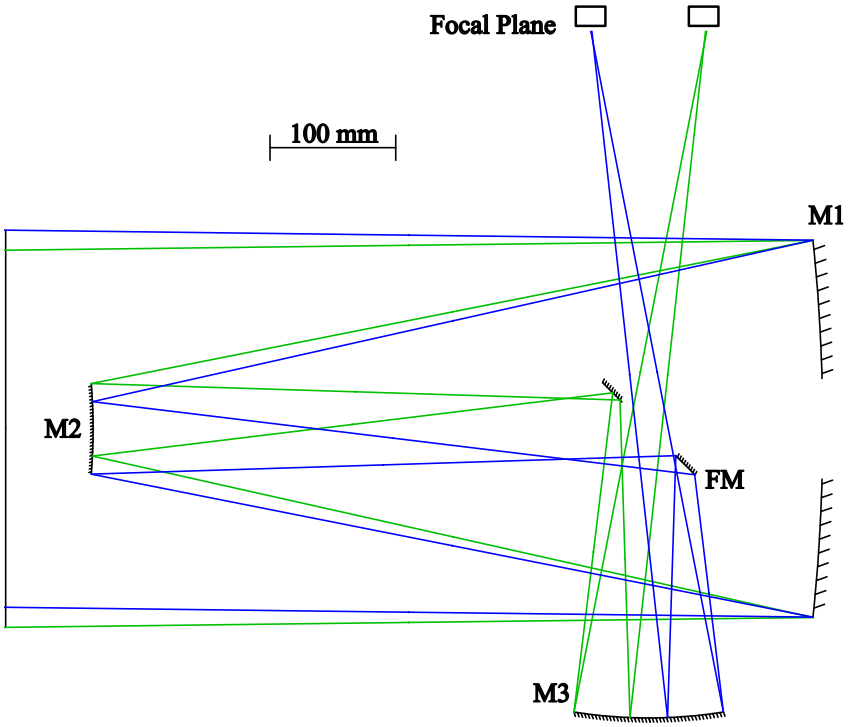

Figure 2. GLADE telescope layout: optical path to the focal plane of rays from fields at $\pm 0^{\circ}.7$ (blue and green lines, respectively).

In fact, the central field is lost at the FM level due to the large central aperture required to allow optical beams from the desired annular field through to the FP. In addition, this is a benefit to our application because the Sun and inner corona, already largely rejected by the external occulter, still provide significant diffracted light, which in GLADE is dumped to space through the FM hole, taking some of the functions of a Lyot stop and/or internal occulter, as shown in Figure 3. Additional features, e.g., a baffling acting as a light trap, are not further addressed in the scope of the present paper.

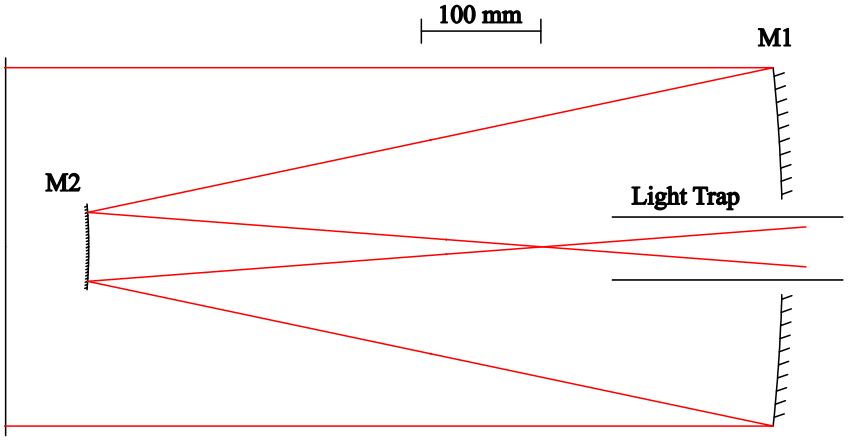

Figure 3. GLADE telescope optical layout: rejection of residual diffracted light from the Sun. Folding mirror FM and subsequent stellar optical paths not shown.

The optical design [23] is derived from a classical Korsch configuration [24,25], further modified to achieve good imaging quality over a large annular field. The focal plane is populated only over a strip ranging from 35′ to 50′, i.e., approximately 0°.58 to 0°.83 (width ∼ 15′), according to the layout shown in Figure 4 (left). The detection system is a set of 12 uniformly spaced $4k \times 4k$ CMOS chips with a pixel size of 4 µm (chip size of 16.4 mm), compatible with current technology (e.g., Teledyne Photometrics (Tucson, AZ) Iris 15 or SBIG (Ottawa, Ontario, Canada) STC-428-P cameras, Sony (https://www.image-sensing-solutions.eu/, accessed on 13 December 2023) IMX455). The well-spaced layout allows for the modular development of simple individual detector modules and also the easing of thermal dissipation issues.

The light deflection values in the GLADE field range between 805 mas at 0°.58 and 562 mas at 0°.83, with an average value of 667 mas at the intermediate 0°.7 radius. Therefore, the deflection amplitude is about two orders of magnitude larger than in Gaia.

The detected signal is somewhat degraded by the finite pixel size, introducing some MTF degradation even on nearly ideal detectors. In Figure 4 (right), the different distributions of photons (solid line), as produced by diffraction in the optical system, and of detected photo-electrons (dashed line) are shown. The effects of a lower peak signal and a wider signal spread are taken into account in the performance assessment.

The effective focal length (EFL) $F = 3.7$ m results in an optical scale $s = 55.75''/\text{mm}$, so that the detector angular size is $0''.22$/pixel and $15'$/chip. The overall sky coverage is 0.77 square degrees. The 10× smaller pixels of GLADE provide a 100× reduction in the background with respect to PROBA3, corresponding to a faint sensitivity improvement of about 5 magnitudes.

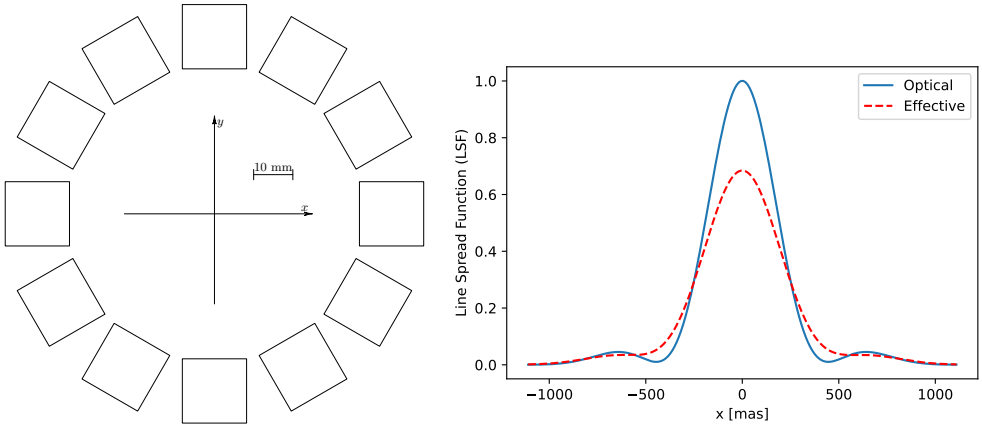

Figure 4. GLADE focal plane (**left**): a ring of 12 $4k \times 4k$ CMOS detectors. Imaging performance (**right**): sections of the optical photon distribution (solid line) and of the effective detected photo-electrons (dashed line).

2.2. Orbit and Operation

The PROBA3 orbit is suited to reasonably efficient observations, covering about 30% of the ecliptic strip during a one year elapse. The chosen orbit is highly elliptical, with 60,530 km apogee and 600 km perigee, and about 59 degree inclination, resulting in an orbital period of 19.7 h. Coronagraphic operation between the precisely aligned spacecraft will take place during the six hours around the apogee.

The whole ecliptic strip may thus be covered in approximately three years. The longer mission lifetime allows for repeat observations, i.e., an increase in the integration time, thus improving the noise performance and/or the calibration accuracy. Further details on the formation flying satellite subsystems and operations are reported in the literature [26–28].

The orbit altitude and/or ellipticity might be modified in order to increase the active observing time fraction above the nominal 6/19.6 h value. However, this trade-off has significant implications for the satellite attitude; it also affects telemetry aspects, changing

the minimum distance (at the perigee) to accessible ground stations. Therefore, such aspects are left to subsequent mission definition study phases.

The apparent displacement of the Sun on the ecliptic is about $0^\circ.986$/day, i.e., $\sim 2''.5$/min. The observation is performed in a step-and-stare mode: pointing on a star field for a while, then moving to keep the (occulted) Sun close to the optical axis. In a simple framework, we can move the pointing direction by $2'$ every 48 min, resetting the Sun position within the $\pm 1'$ range.

During the six-hour eclipses, GLADE observes a sky region approximately $0^\circ.25$ wide along the ecliptic over the $\pm 0^\circ.83$ range covered by the focal plane (Figure 4, left). In practice, the exposure time per star changes depending on position within the field; the average values are considered in the following, leaving detailed analysis to subsequent analyses.

2.3. Error Budget Approach

The performance analysis is based on a simple but realistic model of the instrument and operation and on the deployment of a simulation referred to as the real sky.

The stellar sample used to assess observing performance is derived from the current Gaia DR3 catalog [4], restricted to a $\pm 1^\circ.25$ strip across the ecliptic, down to $G = 16$ mag; the source statistics are shown in Figure 5, evidencing the star density peaks in the intersection with the galactic plane. The nominal GLADE observing region is within $\pm 0^\circ.83$. The star counts from the Gaia DR3 catalog are listed in Table 1; it may be noted that available sources increase rapidly with magnitude.

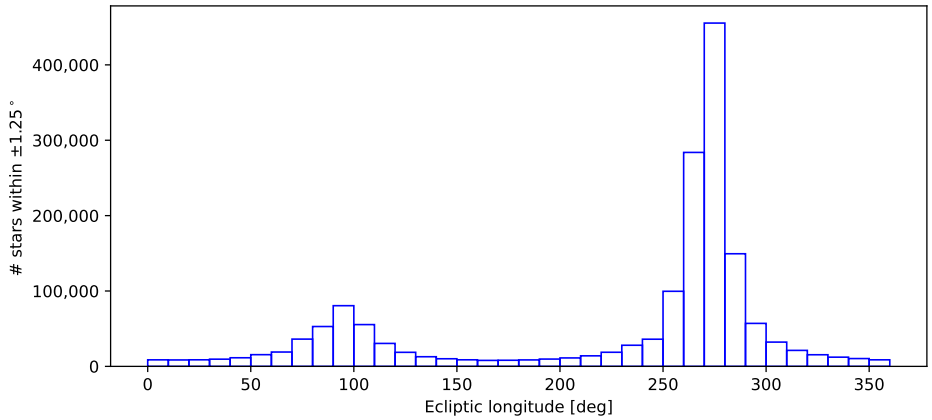

Figure 5. Distribution of stars in a $\pm 1^\circ.25$ strip along the ecliptic; the peaks correspond to the Milky Way intersection regions, respectively, in the Galactic Center (right) and anti-center (left) directions.

Table 1. Observable stars in the ecliptic region from Gaia DR3 catalog in the $\pm 1^\circ.25$ region and in the nominal GLADE field.

Limiting Magnitude	Stars in $\pm 1^\circ.25$	Stars in $\pm 0^\circ.83$
G = 10 mag	8305	5673
G = 11 mag	21,158	14,499
G = 12 mag	52,056	35,740
G = 13 mag	125,335	86,030
G = 14 mag	299,862	206,858
G = 15 mag	703,447	486,903
G = 16 mag	1,609,648	1,117,521

Due to the high-precision measurement goals, it is necessary to thoroughly address both random and systematic errors, respectively, in Sections 2.3.1 and 2.3.2. A full treatment is beyond the scope of this paper; hereafter, we focus on some of the main concepts, in order to illustrate the underlying logic and substantiate the basic principles involved. Several among the instrument and operation parameters, affecting the signal level and astrometric

performance on unresolved objects (stars), are reported in the literature [16,29,30], or scaled according to the current geometry.

2.3.1. Random Errors

In each focal plane image, the source relative positions can be assessed with precision [31] depending on the optical resolution, hence the photon distribution on the focal plane, and on the source brightness, through the signal to noise ratio (S/N). A simple expression for the one-dimensional location uncertainty σ [32] is

$$\sigma = \alpha \frac{\lambda}{D} \cdot \frac{1}{\mathrm{S/N}}, \tag{2}$$

where λ/D is a geometric factor related to diffraction and the ideal telescope resolving power through the observing effective wavelength λ and instrument diameter D. The α parameter is a factor taking into account all other numerical and geometric terms, in particular the pixel size; the above simplified formula is valid over a limited range of the relevant experimental conditions, e.g. away from detector saturation.

The separation between sources is affected by the uncertainty on either end; hence, its precision is mostly limited by the faintest object in the pair.

The location uncertainty is the photon-limited astrometric noise, which must be combined with other random and systematic contributions to achieve a realistic error budget. Some considerations on this issue are addressed below. For practical reasons, namely detector saturation on bright sources, the overall six-hour observation (solid black line) is split into shorter elementary exposures with a nominal duration of one minute (dotted black line). The brightest stars ($G \leqslant 12$ mag) will require further reduction in the elementary exposure time.

2.3.2. Systematic Errors

Systematic errors are induced by our limited knowledge on the system parameters and measurement conditions; in particular, we take into account the simple case of a dominant perturbation on the telescope EFL, affecting the optical scale $s = 1/F$, which translates the actual focal plane estimate of image separation in pixels into the corresponding angular value on the sky. The effect of optical scale variations is a change in the estimated separation between stars, which is directly related to the mission goal, i.e., the determination of the light deflection induced by gravity.

A different source of systematic error is the limited knowledge of actual star parameters within the observed sample. Star positions and parallaxes are affected by uncertainties, which are explicitly listed in the Gaia DR3 (and future DR4) catalog. The GLADE measurement of deflected star positions is therefore jeopardized by both contributions, directly by the former and indirectly by the latter. The relationship between variations in the light deflection effect, namely a change $\delta\gamma$ (in 10^{-5} units) of the γ PPN parameter, and the shift $\delta\varpi$ (in μas) induced in stellar parallaxes [33] (Equation (12) therein) occurs in the case of Gaia (averages on the sky):

$$\frac{\delta\varpi\ [\mu\mathrm{as}]}{\delta\gamma\ [10^{-5}]} \simeq -\frac{1}{35}. \tag{3}$$

Hence, errors on parallaxes could potentially affect the estimate of γ. The origin of the effect may be better perceived by the consideration that it corresponds to a displacement of star images depending on their angular separation from the Sun and distance from the observer, and both factors also relate to light deflection.

This relation between the systematic errors is a direct consequence of Gaia's very specific observational geometry, when variations in the trigonometric parallaxes and PPN gamma have very similar impacts on observables. It is worth emphasizing that no such kind of systematic error can appear in the GLADE experiment because the parallactic and light deflection effects are completely decoupled. Indeed, the parallactic displacement is

toward the Solar System's barycenter, while the deflection effect is directed toward the Sun's center. The angle between these directions can be up to 45 degrees if an object is observed one degree from the Sun.

3. Results

The limiting performance of light deflection measurement by GLADE is related to the photon budget of observable stars and the instrument response, as expounded in Section 3.1. The self-calibration potential of GLADE is preliminarily addressed in Section 3.2, in particular with respect to the discrimination capability between instrument parameters (effective focal length, i.e., optical scale) and the main measurable, that is, the actual value of apparent star displacement. Finally, in Section 3.3, we provide a glimpse of how to cope with potential errors due to uncertainty in the astrometric parameters of the observed stellar sample.

3.1. Photon Limited Performance: Astrometric Noise Level

The nominal S/N (blue line) and related astrometric uncertainty (black lines), respectively, for one minute (elementary exposure, dotted line), one hour (dashed line) and six hours (full eclipse observation, solid line), as a function of magnitude are shown in Figure 6.

Each source in the Gaia catalog may be considered a materialization of the celestial reference system; therefore, the set of relative positions (α_M, δ_M), as measured by GLADE observing around the Sun, may be compared with the expected values (α_E, δ_E) associated to the undeflected (catalog) coordinates, the current pointing (nominally centered on the Sun) and the ideal (GR) value $\gamma = 1$. The comparison allows an assessment of the light deflection discrepancy with respect to GR over the field.

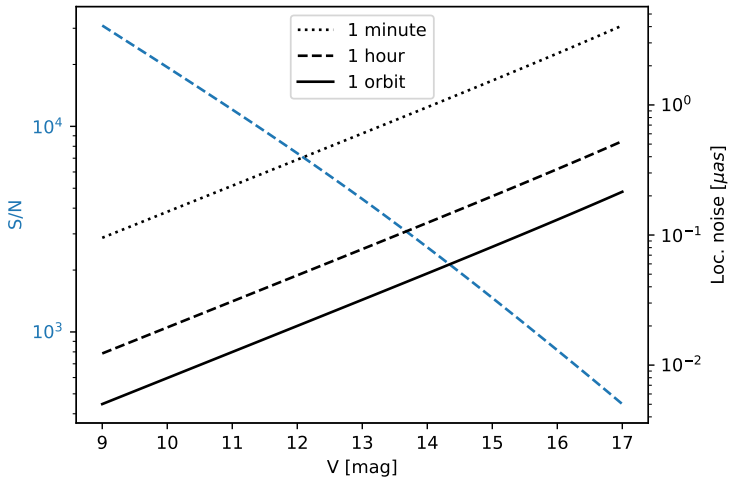

Figure 6. S/N (blue) and astrometric noise level (black) as a function of magnitude. The full orbit (solid line), intermediate (dashed black line) and elementary exposure (dotted line) precision are shown to demonstrate the cumulative measurement contributions.

Each star is located with a precision (Equation (2)) basically related to its magnitude and S/N, whereas the overall reference system for differential astrometry [30] is defined by the whole set of field stars. Reference values of S/N (blue dashed line) and location uncertainty for near solar spectral-type stars are shown in Figure 6, respectively, for a one-minute elementary exposure (dotted black line), an intermediate one-hour period (dashed black line) and the whole six-hour observing time allowed by good alignment with the occulter during one orbit (solid black line). Over the selected magnitude range, the curves do not depart significantly from the photon limit, i.e., the effects of background and readout noise are negligible; detector pixel saturation on one-minute exposures occurs for stars brighter than $G \simeq 11.5$ mag, which will require shorter elementary integration.

The cumulative precision of light deflection increases with the number of measurements throughout the mission's lifetime. The limited duty cycle of observation (6 h in each 19.6 h orbit, ∼30%) requires a three-year mission lifetime to actually cover the full ecliptic strip (minor orbital adjustments may be required to properly phase the observations). The relative cumulative precision in light deflection, or equivalently, in the PPN γ parameter, is shown in Figure 7, respectively, setting a limiting magnitude of $G = 12$ mag (dotted line), $G = 14$ mag (dashed line) and $G = 16$ mag (solid line). Also, the values achieved after relevant time periods are listed, in 10^{-7} units, in Table 2 for the same magnitude range.

Table 2. Mission performance: relative precision, in 10^{-7} units, on the estimate of light deflection.

Limiting Magnitude	0.5 Years	1 Year	2 Years	3 Years
$G = 12$ mag	1.60	1.11	0.787	0.643
$G = 14$ mag	1.49	1.01	0.713	0.582
$G = 16$ mag	1.44	0.94	0.665	0.543

We remark that the actual improvement in precision provided by a large number (Table 1) of comparably faint stars is marginal in spite of their significant impact on system resources (e.g., memory and telemetry). However, their relevance is to be taken into account with respect to accuracy since they allow better calibration and averaging of individual catalog errors. The mission may be further extended (e.g., to five years) to achieve higher precision and, above all, better accuracy, i.e., reliability of the results.

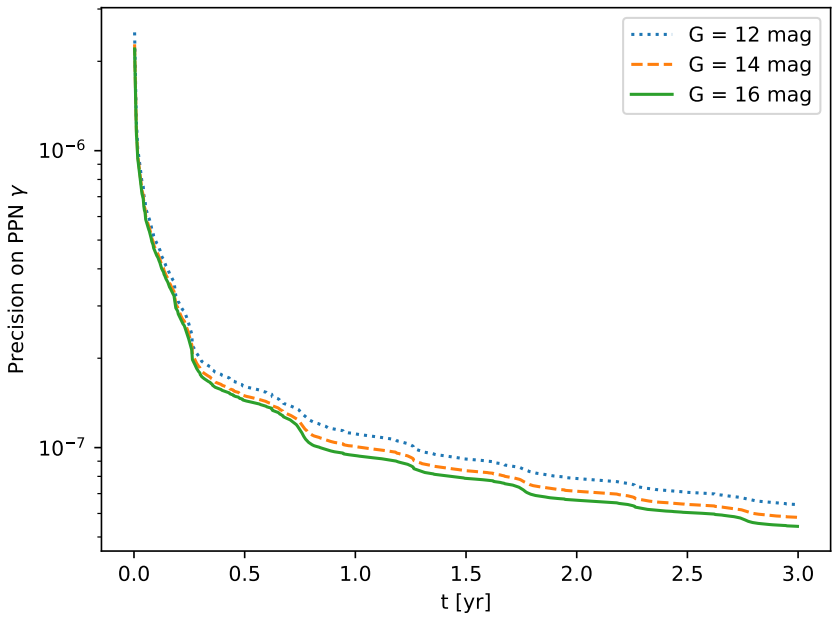

Figure 7. GLADE mission performance over a three-year lifetime.

3.2. Optical Parameter Calibration

The light deflection effect acts purely in the radial direction with respect to the nominal observing geometry and instrument symmetry (e.g., Figure 4). Therefore, the measurement is mostly sensitive to disturbances affecting the radial component of the electro-optical response parameters.

Several optical aberrations have a radial dependence, usually different from that of deflection (Equation (1)). The instrument response may be most effectively calibrated by observation of known stellar fields, e.g., in off-eclipse periods. The concept of relative astrometry calibration is discussed, e.g., in [30], which discusses how the local reference frame, materialized by the observed Gaia DR3 sources, can be consolidated by simple model fitting to the measurements. The basic idea is recalled hereafter.

It is convenient to express positions in terms of local radial and tangential coordinates, respectively, in angular (ρ, τ) and linear (r, t) units. We can rewrite Equation (1) as $\rho_D = \rho + (1+\gamma) f(\rho)$, where ρ is the nominal angle of the star with respect to the current Sun position and ρ_D is the observed (deflected) position, through the PPN parameter γ. Then, a star at angular coordinates (ρ, τ) is projected through the EFL F of an ideal telescope to the linear FP position

$$r = F\rho_D\,, \quad t = F\tau\,. \tag{4}$$

The detected position of a star may be affected, e.g., by a deviation $\delta\gamma$ from unity of the γ parameter or by an EFL variation δF, as

$$r + \delta r = F(1 + \frac{\delta F}{F})(\rho_D + \delta\gamma f(\rho))\,, \quad t + \delta t = F(1 + \frac{\delta F}{F})\tau\,. \tag{5}$$

Therefore, tangential coordinates are basically unaffected by deflection (which is basically radial) and its uncertainty, allowing us to decouple the issue of EFL calibration from the deflection measurement.

The self-calibration potential of GLADE can be glimpsed, e.g., in the case of a focal plane image including N stars, with photo-center estimate errors following the photon-limited astrometric noise described by Equation (2) and shown in Figure 6 at the level of a few 0.1 μas for intermediate exposure and magnitude. The EFL must match the measured and cataloged star positions. It may be noted that catalog errors are systematic on an individual basis, but they act collectively as random errors since each star is affected by its own error within known uncertainty.

We assume a typical catalog position error $\sigma_t \simeq 10\,\mu$as for each of $N \simeq 20$ stars uniformly distributed on any $L = 15'$ chip (typical separation $\Delta\tau \sim 1'$) in average observing conditions. Therefore, the EFL precision on individual field exposures (over a few hours) is of the order of

$$\frac{\sigma(s)}{s} \simeq \frac{\sigma_t}{\Delta\tau} = \simeq 1.7 \times 10^{-7}\,, \tag{6}$$

which is quite adequate to the mission goal, since it is well below the random error on the same time scale (of order 10^{-6}), and it will be further averaged throughout the measurements.

3.3. Catalog Errors

The parallax distribution of the GLADE star sample from Gaia DR3 is shown in Figure 8 (left), together with their current estimated errors (right). It may be noted that most stars have parallaxes of a few mas, i.e., they are in the distance range of a few hundred to a few thousand parsecs; a few cases of negative parallaxes are due to instrumental and model errors still present.

Parallax errors are mostly in the few ten μas range. Assuming it is a totally random distribution, their contribution would be averaged out, i.e., since they are in the order of 10^6 sources, it reduces to the order of a few tens of nano-arcsecs.

Moreover, the scaling factor toward the parallax effect on the light deflection measurement due to the observing geometry is highly favorable (Section 2.3.2), thus reducing the overall effect to the order of one nano-arcsec or below. Taking into account the nominal value of the deflection in the observed region (∼667 mas), the contribution of parallax errors to the GLADE measurement of light deflection is in the 10^{-9} range, i.e., well below the photon-limited performance.

The effects of a systematic error on parallaxes, i.e., the parallax zero point estimated in the Gaia DR3 catalog in ∼17 μas [5], would of course be much more relevant, as they are not averaged by many observations. The limitations to light deflection measurement would therefore only be mitigated by the observing geometry to the order of 10^{-6}. However, we expect that future releases of the Gaia catalog (DR4) will significantly improve on the parallax zero point. The issue might be further mitigated, e.g., by dedicated observations (by GLADE itself or other instruments) providing better parallax determinations, at least for part of the sample.

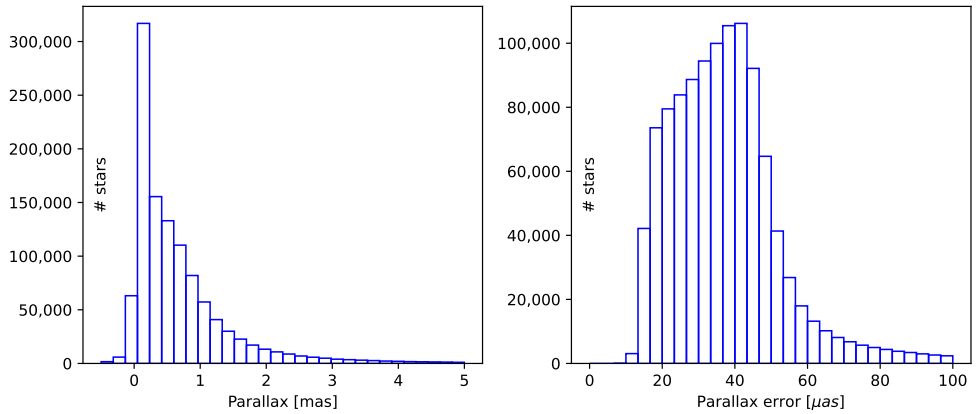

Figure 8. Distribution of star parallaxes and parallax errors from Gaia DR3 in the $\pm 0^{\circ}.84$ ecliptic latitude strip observed by GLADE.

4. Discussion

The proposed GLADE mission concept builds on proven concepts and achieves performance comparable to that of much more challenging designs previously submitted to M3 and M4 ESA calls.

It may be noted that the achievable precision (Figure 7) is a performance indication related to the light deflection measurement, even if, for short, it is referred to as the PPN parameter γ. At this level, the relevance of the PPN model itself may be questioned, and more detailed (e.g., parametrized post-post-Newtonian (PPPN)) interpretation models may be called for. In that case, the $<10^{-7}$ precision is spread among the different estimated parameters.

In addition, light deflection is described throughout this paper as having a simple circular symmetry, which is not necessarily the case for all possible gravitation models. Also, deviations from circular symmetry might be induced in cases of violation of the Lorentz invariance [34]. GLADE is a convenient platform for the detection of such kinds of effects due to its principle of simultaneous measurement over a corona around the Sun.

The GLADE concept is intrinsically compatible with a solar science payload, given the common observing region. The multiple payload observation is a common approach in this context, used in previous missions, e.g., SOHO [35]. In practice, a common external occulter may feed several instruments observing the Sun and circumsolar regions at different radii, in different spectral bands and with various spectroscopic and polarimetric capabilities. Future project development is therefore also a matter of negotiation among scientific communities interested, respectively, in fundamental physics, solar physics and space weather.

The proposed implementation based on a 0.3 m telescope may be considered as an intermediate-scale version of the experiment, roughly corresponding to a medium-class mission on the instrument side (i.e., factoring out the occulter and formation flying aspects). It can be shown that a comparably limited upgrade of the instrument, switching to a one-meter-class telescope and corresponding detection system (at an order of 30 chips with comparable specifications), will provide a remarkable performance boost. In fact, the telescope diameter D affects both imaging resolution in diffraction-limited conditions, decreasing at $1/D$, and S/N, increasing with D in photon-limited conditions; therefore, the location uncertainty from Equation (2) scales as D^{-2}.

This provides an overall improvement on light deflection determination, all other factors left unchanged, by about one order of magnitude, pushing the photon-limited precision level in the same mission lifetime below 10^{-8}.

5. Conclusions

We propose a novel concept for the implementation of the classical test of general relativity related to light bending around the Sun, which may allow for discrimination among competing theories of gravitation at the 10^{-7} level or better. The key technology of an external occulter in formation flying, generating an artificial long-lasting eclipse, shall be demonstrated by the forthcoming ESA mission PROBA3. The measurement concept, also thanks to the circular symmetry enforced into the design, is robust with respect to rejection and/or calibration of instrumental and external disturbances, including uncertainty on the position and parallax of observed sources. The main instrument is a small telescope (0.3 m diameter) with an annular field of view at $\sim 0^{\circ}.7$ from the Sun, performing high-precision astrometry on comparably bright stars $G \leqslant 16$ mag. By simulating the real sky distribution of observable stars down to $G = 16$ mag, we figure out that the proposed GLADE setup, over a mission lifetime of three years, will be able to achieve a relative precision of light deflection of $\sim 5 \times 10^{-8}$. A moderate increase in the instrument size by a factor of three may provide a performance improvement of one order of magnitude.

Author Contributions: Conceptualization, M.G. and A.V.; methodology, M.G., A.R. and F.L.; software, A.V. and M.G.; validation, M.G., A.V. and A.G.B.; formal analysis, A.V. and A.G.B.; investigation, M.G., A.R. and D.B.; resources, M.G. and A.R.; data curation, A.V., F.L. and M.G.; writing—original draft preparation, M.G., A.V. and A.G.B.; writing—review and editing, D.B., F.L. and A.R.; visualization, M.G. and D.B.; supervision, M.G.; project administration, A.R.; funding acquisition, M.G. and A.R. All authors have read and agreed to the published version of the manuscript.

Funding: This research was funded by the Agenzia Spaziale Italiana (ASI) through contract 2018-24-HH.0 and its Addendum 2018-24-HH.1-2022 to the Italian Istituto Nazionale di Astrofisica (INAF).

Data Availability Statement: Astrophysical data for the performance simulation are derived from the publicly available Gaia catalog (DR3). Optical design data of the telescope will be detailed in a forthcoming paper. Intermediate and final results of our simulation will be made available (within reason) upon request.

Acknowledgments: We gratefully acknowledge the contribution of M. Lattanzi to the development of the idea of a modern rendition of the 1919 Eddington, Dyson and Davidson eclipse experiment. Many other scientists helped our understanding of the scientific and practical issues involved and eventually to the currently proposed solution.

Conflicts of Interest: The authors declare no conflicts of interest. The funders had no role in the design of the study; in the collection, analyses, or interpretation of data; in the writing of the manuscript; or in the decision to publish the results.

Abbreviations

The following abbreviations are used in this manuscript:

ASPIICS	Association de Satellites Pour l'Imagerie et l'Interférométrie de la Couronne Solaire
CMOS	Complementary metal–oxide semiconductor
DR3	Data Release 3
FM	Folding mirror
FP	Focal plane
GLADE	Gravitational Light-bending Astrometry Dual-satellite Experiment
GR	General relativity
M1	Primary mirror
M2	Secondary mirror
M3	Tertiary mirror
PPN	Parametrized post-Newtonian
PPPN	Parametrized post-post-Newtonian
PROBA3	Project for On-Board Autonomy-3

References

1. Will, C.M. The Confrontation between General Relativity and Experiment. *Living Rev. Relativ.* **2006**, *9*, 3. [CrossRef] [PubMed]
2. Bertotti, B.; Iess, L.; Tortora, P. A test of general relativity using radio links with the Cassini spacecraft. *Nature* **2003**, *425*, 374–376. [CrossRef] [PubMed]
3. Gaia Collaboration; Prusti, T.; de Bruijne, J.H.J.; Brown, A.G.A.; Vallenari, A.; Babusiaux, C.; Bailer-Jones, C.A.L.; Bastian, U.; Biermann, M.; Evans, D.W.; et al. The Gaia mission. *Astron. Astrophys.* **2016**, *595*, A1. [CrossRef]
4. Gaia Collaboration. Gaia Early Data Release 3. Summary of the contents and survey properties. *Astron. Astrophys.* **2021**, *649*, A1. [CrossRef]
5. Lindegren, L.; Klioner, S.A.; Hernández, J.; Bombrun, A.; Ramos-Lerate, M.; Steidelmüller, H.; Bastian, U.; Biermann, M.; de Torres, A.; Gerlach, E.; et al. Gaia Early Data Release 3—The astrometric solution. *Astron. Astrophys.* **2021**, *649*, A2. [CrossRef]
6. Hobbs, D.; Holl, B.; Lindegren, L.; Raison, F.; Klioner, S.; Butkevich, A. Determining PPN γ with Gaia's astrometric core solution. In *Proceedings of the Relativity in Fundamental Astronomy: Dynamics, Reference Frames, and Data Analysis*; Klioner, S.A., Seidelmann, P.K., Soffel, M.H., Eds.; Cambridge University Press: Cambridge, UK, 2010; Volume 261, pp. 315–319. [CrossRef]
7. Vecchiato, A.; Lattanzi, M.G.; Bucciarelli, B.; Crosta, M.; de Felice, F.; Gai, M. Testing general relativity by micro-arcsecond global astrometry. *Astron. Astrophys.* **2003**, *399*, 337–342. [CrossRef]
8. Ashby, N. Relativity in the Global Positioning System. *Living Rev. Relativ.* **2003**, *6*, 1. [CrossRef]
9. Ashby, N.; Nelson, R.A. GPS, Relativity, and Extraterrestrial Navigation. *Iau Symp.#261 Am. Astron.* **2009**, *41*, 889.
10. Misner, C.W.; Thorne, K.S.; Wheeler, J.A. *Gravitation*; W.H. Freeman and Co.: San Francisco, CA, USA, 1973.
11. Damour, T.; Nordtvedt, K. General relativity as a cosmological attractor of tensor-scalar theories. *Phys. Rev. Lett.* **1993**, *70*, 2217–2219. [CrossRef]
12. de Bernardis, P.; Ade, P.A.R.; Bock, J.J.; Bond, J.R.; Borrill, J.; Boscaleri, A.; Coble, K.; Crill, B.P.; De Gasperis, G.; Farese, P.C.; et al. A flat Universe from high-resolution maps of the cosmic microwave background radiation. *Nature* **2000**, *404*, 955–959. [CrossRef]
13. Hinshaw, G.; Larson, D.; Komatsu, E.; Spergel, D.N.; Bennett, C.L.; Dunkley, J.; Nolta, M.R.; Halpern, M.; Hill, R.S.; Odegard, N.; et al. Nine-year Wilkinson Microwave Anisotropy Probe (WMAP) Observations: Cosmological Parameter Results. *Astrophys. J. Suppl.* **2013**, *208*, 19. [CrossRef]
14. Planck Collaboration; Ade, P.A.R.; Aghanim, N.; Armitage-Caplan, C.; Arnaud, M.; Ashdown, M.; Atrio-Barandela, F.; Aumont, J.; Baccigalupi, C.; Banday, A.J.; et al. Planck 2013 results. XVI. Cosmological parameters. *Astron. Astrophys.* **2014**, *571*, A16. [CrossRef]
15. Di Valentino, E.; Melchiorri, A.; Silk, J. Planck evidence for a closed Universe and a possible crisis for cosmology. *Nat. Astron.* **2020**, *4*, 196–203. [CrossRef]
16. Gai, M.; Vecchiato, A.; Ligori, S.; Sozzetti, A.; Lattanzi, M.G. Gravitation astrometric measurement experiment. *Exp. Astron.* **2012**, *34*, 165–180. [CrossRef]
17. Vecchiato, A.; Fienga, A.; Gai, M.; Lattanzi, M.G.; Riva, A.; Busonero, D. Astrometric Gravitation Probe: a space mission concept for fundamental physics. *Iau Gen. Assem.* **2015**, *29*, 2247746.
18. Kataoka, R.; Shiota, D.; Fujiwara, H.; Jin, H.; Tao, C.; Shinagawa, H.; Miyoshi, Y. Unexpected space weather causing the reentry of 38 Starlink satellites in February 2022. *J. Space Weather Space Clim.* **2022**, *12*, 41. [CrossRef]
19. Cliver, E.W.; Dietrich, W.F. The 1859 space weather event revisited: limits of extreme activity. *J. Space Weather Space Clim.* **2013**, *3*, A31. [CrossRef]
20. Shestov, S.V.; Zhukov, A.N.; Inhester, B.; Dolla, L.; Mierla, M. Expected performances of the PROBA-3/ASPIICS solar coronagraph: Simulated data. *Astron. Astrophys.* **2021**, *652*, A4. [CrossRef]
21. Lindegren, L. Photoelectric astrometry—A comparison of methods for precise image location. In Proceedings of the IAU Colloq. 48: Modern Astrometry, Vienna, Austria, 12–14 September 1978; Prochazka, F.V., Tucker, R.H., Eds.; pp. 197–217. Available online: https://www.researchgate.net/profile/Lennart-Lindegren/publication/234362654_Photoelectric_astrometry_-_A_comparison_of_methods_for_precise_image_location/links/5612aa6b08ae83674f43927a/Photoelectric-astrometry-A-comparison-of-methods-for-precise-image-location.pdf (accessed on 13 December 2023).
22. Espinosa, S.; Silva, J.F.; Mendez, R.A.; Lobos, R.; Orchard, M. Optimality of the maximum likelihood estimator in astrometry. *Astron. Astrophys.* **2018**, *616*, A95. [CrossRef]
23. Riva, A.; Gai, M.; Vecchiato, A.; Busonero, D.; Lattanzi, M.; Landini, F.; Qi, Z.; Tang, Z. RAFTER: Ring Astrometric Field Telescope for Exo-planets and Relativity. In Proceedings of the Society of Photo-Optical Instrumentation Engineers (SPIE) Conference Series, online, 14–18 December 2020; Volume 11443, p. 11443. [CrossRef]
24. Korsch, D. Anastigmatic three-mirror telescope. *Appl. Opt.* **1977**, *16*, 2074–2077. [CrossRef]
25. Korsch, D. Design and optimization technique for three-mirror telescopes. *Appl. Opt.* **1980**, *19*, 3640–3645. [CrossRef] [PubMed]
26. Galy, C.; Thizy, C.; Stockman, Y.; Galano, D.; Rougeot, R.; Melich, R.; Shestov, S.; Landini, F.; Zukhov, A.; Kirschner, V.; et al. Straylight analysis on ASPIICS, PROBA-3 coronagraph. In Proceedings of the International Conference on Space Optics—ICSO 2018, Chania, Greece, 9–12 October 2018; Sodnik, Z., Karafolas, N., Cugny, B., Eds.; Volume 11180, p. 111802H. [CrossRef]
27. Loreggia, D.; Fineschi, S.; Capobianco, G.; Bemporad, A.; Casti, M.; Landini, F.; Nicolini, G.; Zangrilli, L.; Massone, G.; Noce, V.; et al. PROBA-3 mission and the Shadow Position Sensors: Metrology measurement concept and budget. *Adv. Space Res.* **2021**, *67*, 3793–3806. [CrossRef]

28. Capobianco, G.; Amadori, F.; Fineschi, S.; Bemporad, A.; Casti, M.; Loreggia, D.; Noce, V.; Pancrazzi, M.; Landini, F.; Thizy, C.; et al. Formation flying performances simulator for the shadow position sensors of the ESA PROBA-3 mission. In Proceedings of the International Conference on Space Optics—ICSO 2020, Online, 30 March–2 April 2021; Cugny, B., Sodnik, Z., Karafolas, N., Eds.; 2021; Volume 11852, p. 118526P. [CrossRef]
29. Gai, M.; Busonero, D.; Cancelliere, R. Performance of an Algorithm for Estimation of Flux, Background, and Location on One-dimensional Signals. *Publ. Astron. Soc. Pac.* **2017**, *129*, 054502. [CrossRef]
30. Gai, M.; Vecchiato, A.; Riva, A.; Butkevich, A.G.; Busonero, D.; Qi, Z.; Lattanzi, M.G. Relative Astrometry in an Annular Field. *Publ. Astron. Soc. Pac.* **2022**, *134*, 035001. [CrossRef]
31. Mendez, R.A.; Silva, J.F.; Orostica, R.; Lobos, R. Analysis of the Cramér-Rao Bound in the Joint Estimation of Astrometry and Photometry. *Publ. Astron. Soc. Pac.* **2014**, *126*, 798. [CrossRef]
32. Lindegren, L.; Perryman, M.A.C. GAIA: Global astrometric interferometer for astrophysics. *Astron. Astrophys.* **1996**, *116*, 579–595. [CrossRef]
33. Butkevich, A.G.; Vecchiato, A.; Bucciarelli, B.; Gai, M.; Crosta, M.; Lattanzi, M.G. Post-Newtonian gravity and Gaia-like astrometry. Effect of PPN γ uncertainty on parallaxes. *Astron. Astrophys.* **2022**, *663*, A71. [CrossRef]
34. Tso, R.; Bailey, Q.G. Light-bending tests of Lorentz invariance. *Phys. Rev. D* **2011**, *84*, 085025. [CrossRef]
35. Domingo, V.; Fleck, B.; Poland, A.I. The SOHO Mission: an Overview. *Sol. Phys.* **1995**, *162*, 1–37. [CrossRef]